THE JOURNAL OF PHYSICAL CHEMISTRY LETTERS
A JOURNAL OF THE AMERICAN CHEMICAL SOCIETY

pubs.acs.org/JPCL Letter

Mode-Specific Autodetachment Dynamics of an Excited Non-valence Quadrupole-Bound State

Do Hyung Kang, Jinwoo Kim, Min Cheng, and Sang Kyu Kim*

Cite This: J. Phys. Chem. Lett. 2021, 12, 1947−1954 Read Online

ACCESS | Metrics & More | Article Recommendations | Supporting Information

ABSTRACT: The autodetachment dynamics of vibrational Feshbach resonances of the quadrupole-bound state (QBS) for the first time has been investigated in real time for the first excited state of the 4-cyanophenoxide (4-CP) anion. Individual vibrational resonances of the cryogenically cooled 4-CP QBS have been unambiguously identified, and their autodetachment rates state-specifically measured using the picosecond time-resolved pump−probe technique employing the photoelectron velocity-map imaging method. The autodetachment lifetime (τ) is found to be strongly dependent on mode, giving τ values of ∼56, ∼27, and ≤2.8 ps for the $12'^1$ (E_{vib} = 406 cm^{-1}), $12'^2$ (E_{vib} = 806 cm^{-1}), and $21'^1$ (E_{vib} = 220 cm^{-1}) modes, respectively. The striking mode-specific behavior of the QBS lifetime has been invoked by the physical model in which the loosely bound electron falls off by the dynamic wobbling of the three-dimensional quadrupole moment ellipsoid associated with the corresponding vibrational motion in the autodetachment process.

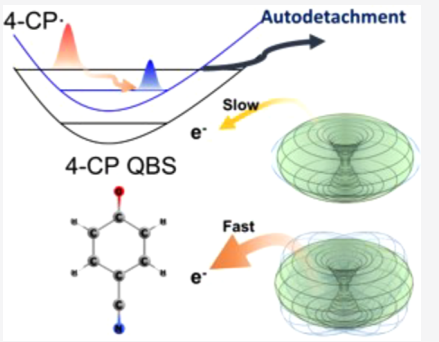

The long-range potential between the electron and neutral core reveals the anionic state has a loosely bound electron with a low binding energy.[1−3] This so-called anionic non-valence bound state is ubiquitous in chemistry and biology, playing an important role in formation of the interstellar anion species[4−6] or electron-mediated biological information transfer.[7,8] The dipole-bound state (DBS), among many different non-valence bound states, has been both intensively and extensively interrogated over the past several decades.[9−13] It has become a rule of thumb that the DBS should exist whenever the dipole moment of the neutral core exceeds ∼2.5 D.[14−16] Naturally, the DBS has been found in many different chemical systems, providing essential dynamic information about the nature of the long-range force governing the attachment or detachment of the electron.[17−22] It is noteworthy that a recent series of outstanding studies of the DBS of the cryogenically cooled anions, pioneered by the Wang group,[23] have allowed the unprecedented identification of many well-resolved vibrational Feshbach resonances of various chemical systems, giving us a great opportunity to unravel the quantum-mechanical nature of such resonances below or above the photodetachment threshold.[24−29] It is also quite notable that the state-specific real-time autodetachment dynamics of the DBS for the first time has been reported for the phenoxide anion very recently.[30] The picosecond time-resolved pump−probe technique applied on the cryogenically cooled anion species (Figure 1) turns out to be extremely powerful in the investigation of the quantum nature of the Feshbach resonances.

Compared to the DBS, other non-valence anionic states such as the correlation-bound state (CBS) or quadrupole-bound state (QBS) have been relatively less studied to date. Although distinctly classifying the prevalence of any particular long-range force acting in the specific non-valence bound anions seems to be a nontrivial task,[3,31,32] there have been quite a few successful experimental and theoretical studies regarding the CBS[33−38] and QBS.[2,39−44] The most definitive experimental example of the QBS, for instance, seems to be the case of the *trans*-succinonitrile anion.[45,46] Using high-resolution photoelectron spectroscopy and theoretical calculations, the origin of the small binding energy of ∼20 meV of the *trans*-succinonitrile anion has been ascribed to the electron-quadrupolar interaction. A recent study of the cryogenically cooled 4-cyanophenoxide (4-CP) anion,[47] on the contrary, provides the first example of the excited QBS anion. The 4-CP radical consists of two opposing electron-withdrawing substituents of O· and CN on the phenyl moiety. This specific molecular geometry gives an extremely tiny dipole moment of ∼0.3 D. On the contrary, the dipolar property of the 4-CP radical imposes a somewhat large quadrupole moment (QM), giving the following traceless diagonal matrix elements: Q_{xx} = −20.5321 D Å, Q_{yy} = 15.1042 D Å, and Q_{zz} = 5.4279 D Å. According to a recent report,[47] the photodetachment threshold of the 4-CP anion has been found to be 24927

Received: January 18, 2021
Accepted: February 12, 2021

https://dx.doi.org/10.1021/acs.jpclett.1c00169
J. Phys. Chem. Lett. 2021, 12, 1947−1954

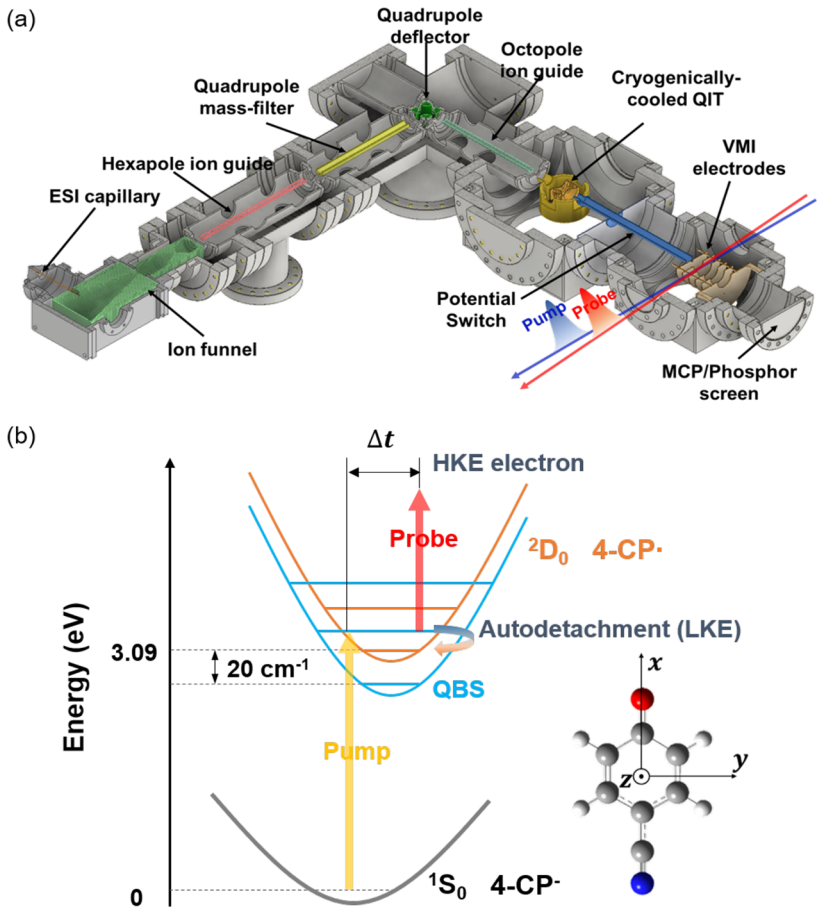

Figure 1. (a) Electrospray ionization (ESI)−photoelectron imaging apparatus combined with the cryogenically cooled quadrupole ion trap (QIT). (b) Energetic diagram of the 4-CP QBS and picosecond time-resolved photoelectron imaging. The 4-CP radical and its molecule-fixed axes are depicted in the inset.

cm^{-1} whereas the binding energy of the excited QBS is estimated to be ∼20 cm^{-1}. The non-valence anionic state of the 4-CP anion with the tiny dipole moment but the large quadrupole moment, therefore, is considered to be the first example of the excited QBS. Herein, using the picosecond time-resolved pump−probe scheme combined with the photoelectron velocity-map imaging setup (Figure 1), we have interrogated the temporal dynamics of the QBS of the cryogenically cooled anion for the first time. The state-specific temporal dynamics of individual Feshbach resonances found above the photodetachment threshold is thoroughly investigated. As no experimental data on the QBS dynamics are available at present, our experiment provides a great opportunity to unravel the underlying physical principles behind the fate of the loosely bound electron in the QBS where the electron is only loosely bound through the electron-QM long-range potential for the first time.

Our photodetachment spectrum taken by detecting the total photoelectron yield from the cryogenically cooled 4-CP anion as a function of the wavelength of the picosecond laser pulse ($\Delta t \sim 1.8$ ps; $\Delta\nu \sim 20$ cm^{-1}) gives the well-resolved vibrational Feshbach resonances of the QBS on the top of the direct photoelectron signal of the featureless background (Figure 2a). The whole spectral feature is quite consistent with that obtained by the nanosecond laser pulse in ref 47, except that the bandwidth of each resonance is quite broadened mostly due to the intrinsic broad bandwidth of the picosecond pump laser pulse.[30] The progression of the 12′ mode stands out, reflecting the geometrical change of the 4-CP anion upon photodetachment.[47] The zero-point level of the QBS, which is supposed to lie ∼20 cm^{-1} below the photodetachment threshold, is also identified, although it is found to be not as distinct as that reported in ref 47 due to the wide energetic window of the picosecond laser pulse. The vibrational Feshbach resonances of the 4-CP QBS are spectrally congested due to the large number of Franck−Condon active vibrational modes, and thus, only a few vibrational bands have been clearly identified as specific normal modes. Nevertheless, the picosecond time-resolved real-time dynamics could be successfully investigated for several well-identified vibrational bands of the QBS above the photodetachment threshold (Figure 2). These bands are $21'^1$, $12'^1$, $12'^1 33'^2/31'^1 33'^1$, and $12'^2$ modes at internal energies of 220, 406, 707, and 806 cm^{-1}, respectively.

Photoelectron velocity-map images taken at these bands give their quantum characteristics as well as the selection rules involved in the autodetachment process (Figure 2b, left). The direct or indirect photodetachment channel could be unambiguously separated out by comparison of photoelectron images taken at resonance bands with those taken at adjacent off-resonances.[26] The indirect autodetachment process obeys the vibrational propensity rule of $\Delta\nu = -1$.[48,49] For the vibrational band at 707 cm^{-1} that was previously assigned as two different combination modes of $12'^1 33'^2/31'^1 33'^1$, the indirect detachment channel leading to the radical with the 31^1 ($-33'^1$) mode is found to be predominant whereas the other channel giving the radical with the 33^2 ($-12'^1$) mode

https://dx.doi.org/10.1021/acs.jpclett.1c00169
J. Phys. Chem. Lett. 2021, 12, 1947−1954

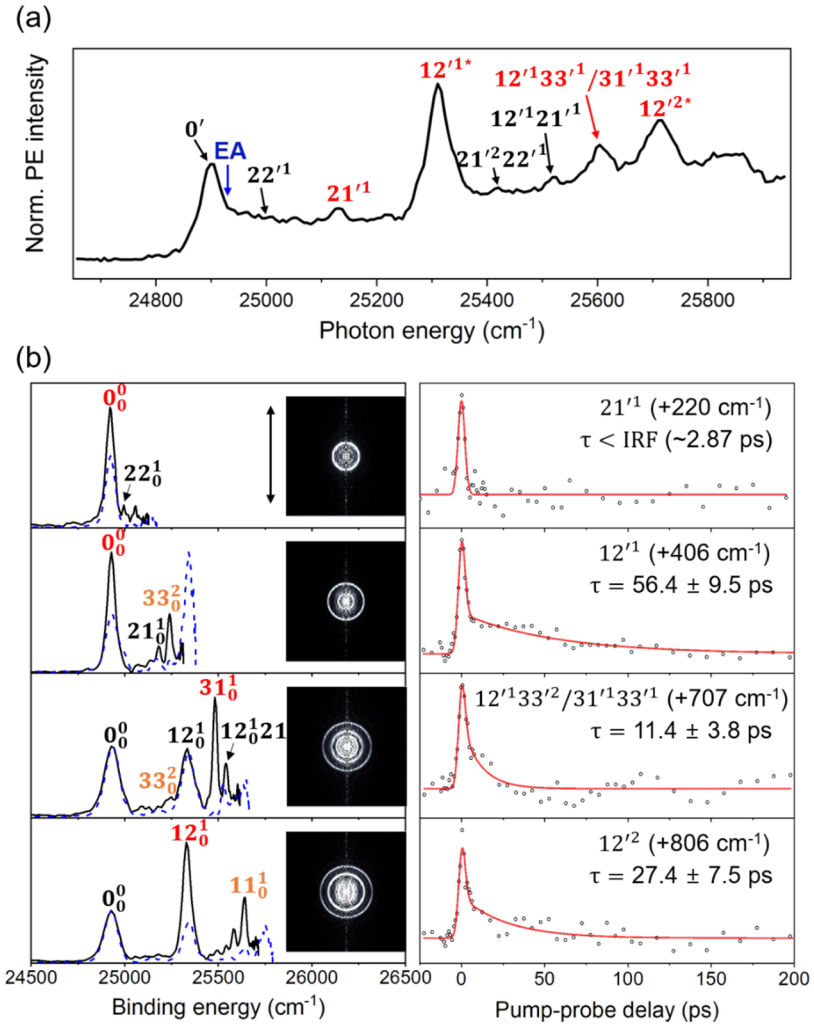

Figure 2. (a) Picosecond photodetachment spectrum of the 4-CP anion. Time-resolved photoelectron images were taken for the peaks labeled in red. An asterisk denotes that the corresponding bands are partly contaminated by the other adjacent weak vibrational modes. (b) Picosecond photoelectron spectra (left) at individual vibrational resonances with corresponding photoelectron images. Photoelectron spectra taken at the nearby off-resonance positions (blue dashed line) are compared with those taken at resonances (black solid lines). Vibrational bands labeled in red show the large enhancement under the resonance condition, whereas those labeled in orange reflect the minor channels due to either the vibronic coupling or spectral contamination. The laser polarization axis is along the vertical direction. Time-resolved photoelectron transients (right) of the 4-CP QBS taken at the Feshbach resonances. Transients have been fitted to obtain the time constants for the single-exponential decay functions (see the Supporting Information). The intensity axes were reversed to show the population decay of the vibrational Feshbach resonances.

excitation is only weakly allowed (*vide infra*). Although it is plausible that the 12′ progression bands may have a contribution from adjacent weak vibrational modes,[47] it is confirmed from the photoelectron spectra that the corresponding autodetachment processes are mainly mediated via the 12′ mode of the QBS (Figure 2).

Now, we measured the autodetachment rate of the vibrational Feshbach resonances by employing the picosecond time-resolved photoelectron imaging scheme (Figure 1b). The wavelength-tuned pump pulse was used to populate the specific vibrational state of QBS, whereas the time-delayed probe laser pulse of 1.57 eV was given to depopulate the corresponding state by the further excitation to the upper detachment continuum, liberating the electron with a high kinetic energy. To measure the autodetachment lifetime, we monitored the depletion and recovery of the photoelectron of the autodetachment process only. This could be achieved by masking the outer part of the phosphor screen so that only the low-kinetic energy photoelectron corresponding to the inner part of photoelectron images could be monitored (*vide infra*).[30] The photoelectron transients then were recorded by scanning the temporal delay between the pump and probe pulses. All of the transients in Figure 2b show the Gaussian-shaped peaks at time zero followed by the single-exponential decays. The Gaussian-shaped peaks with the cross-correlation width should come from the multiphoton and/or strong-field effect as the pump and probe pulses are spatiotemporally overlapped quite perfectly at the zero-time delay. The subsequent single-exponential decays of the transients represent the autodetachment lifetimes of individual Feshbach resonances. The transient of the most prominent $12'^1$ (406 cm^{-1}) band gives an autodetachment lifetime (τ) of 56.4 ± 9.5 ps. This is the first experimental measurement of the QBS vibrational autodetachment rate, which is interestingly ~1.68-fold slower than the comparable $11'^1$ mode of the phenoxide DBS (τ = 33.5 ± 3 ps) (*vide infra*).[30] The transient of the $12'^2$ overtone band (806 cm^{-1}) gives a τ of 27.4 ± 7.5 ps, which is 2 times shorter than that of the $12'^1$ mode. Interestingly, we

https://dx.doi.org/10.1021/acs.jpclett.1c00169
J. Phys. Chem. Lett. 2021, 12, 1947−1954

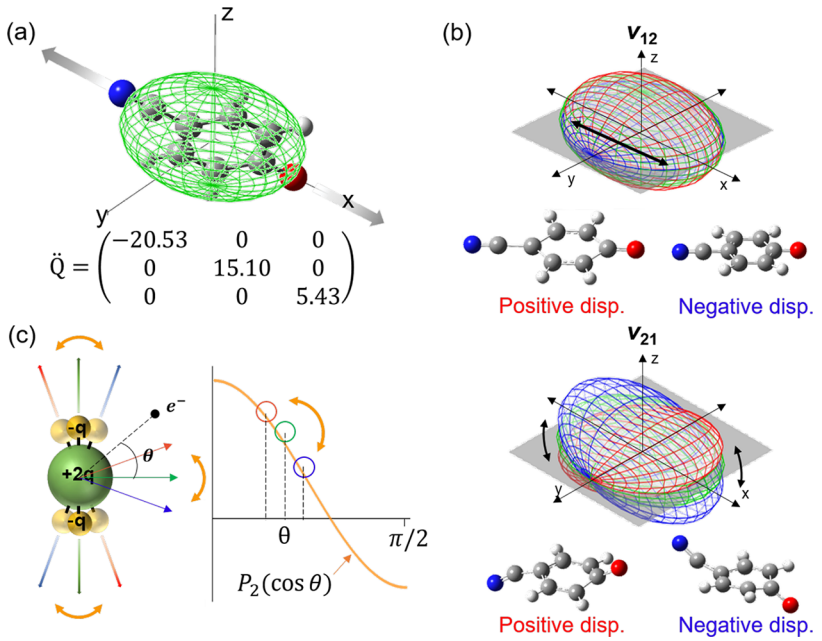

Figure 3. (a) Traceless quadrupole moment tensor of the 4-CP· radical and corresponding three-dimensional QM ellipsoid. Two antiparallel oriented dipolar groups (-CN and -O·) are depicted as gray arrows. (b) Schematics of the QM ellipsoid oscillation of the 4-CP· radical by the (top) ν_{12} or (bottom) ν_{21} mode excitation. The QM ellipsoid of the equilibrium geometry is colored green, while the ellipsoids at positive and negative displacements are colored red and blue, respectively. The geometries of the 4-CP· radical at the positive and negative displacements are also shown as skeletal structures. The ν_{12} mode induces the oscillation along the *x*-axis mainly, resulting in the radial fluctuation of the QM ellipsoid. On the contary, the oscillations of the QM ellipsoid in both angular and radial directions are activated by ν_{21} mode excitation. (c) Schematic diagram (left) of the angular motion of the linear quadrupole showing the instant change of the angle between the electron and linear quadrupole axis. Electron QM potential (right) as a function of the polar angle. The electron positioned at the arbitrary angle (θ) at the equilibrium geometry (green), for instance, experiences the sharply varying electron−QM interaction potential during the angluar distortion following the trace of the second-order Legendre polynomial. The positive and negative displacements are colored red and blue, respectively.

found a dramatic mode-dependent QBS autodetachment lifetime τ of ≤2.87 ps at the $21'^1$ mode. Considering the fact that the internal energy of 220 cm^{-1} at the $21'^1$ mode is much smaller than that of 406 cm^{-1} at the $12'^1$ mode, it is quite remarkable that the autodetachment rate of the $21'^1$ mode is ∼19 times faster than that of the $12'^1$ mode. This strongly indicates that the QBS autodetachment dynamics should be dictated by the topological properties of the particular vibrational modes rather than their energetic scalar properties. In general, as the dynamic range of the QM fluctuation by any specific vibrational mode is larger, the corresponding fluctuation of the long-range potential seems to be more efficient in releasing the loosely bound electron.[50] However, the more evolved stereodynamic aspect should be taken into account to understand the QBS autodetachment dynamics (*vide infra*).

Fermi's golden rule is extremely useful for the quantitative description of the autodetachment rate ($k = \tau^{-1}$).[51,52]

$$k = \frac{2\pi}{\hbar} |\langle \phi_f | W | \phi_i \rangle|^2 \rho(KE_e) \tag{1}$$

where ϕ_i and ϕ_f are the initial and final state wave functions, respectively, W is the coupling operator between the two states, and ρ is the density of states (DOS) of the ejecting electron. The coupling term in eq 1 could be expressed as follows.[52−54]

$$\langle \phi_f | W | \phi_i \rangle = -\frac{\hbar^2}{2m} \left\langle v_f \left| F(q) \frac{\partial}{\partial q} \right| v_i \right\rangle \tag{2}$$

$$F(q) = \frac{1}{\varepsilon_{if}} \left\langle e_f \left| \left(\frac{\partial U}{\partial q} \right) \right| e_i \right\rangle \tag{3}$$

where ε_{if} is the change in the nuclear kinetic energy, q is the normal mode coordinate, and U is the electron binding potential. For the DBS, as the $\frac{\partial U}{\partial q}$ term is proportional to the derivative of the dipole moment (μ) with respect to the normal mode coordinate (q), $(\frac{\partial \mu}{\partial q})$, the IR intensity of the specific normal mode could be successfully invoked for the interpretation of the mode-dependent autodetachment rates.[29,30,55] While the "wobbling" nature of the vibrational mode excitation in the release of the electron[52] could also be applicable to the QBS autodetachment dynamics, it should be emphasized that the nature of the long-range force in the QBS should be quite different from that of the DBS. If one confines the long-range force of the excited state of the 4-CP anion to the potential energy between the electron and QM only, the derivative of the potential energy function with respect to the normal mode could be depicted as follows for the simplest case.

$$\frac{\partial U}{\partial q} = \frac{2e}{4\pi\varepsilon_0} \left[\frac{\partial}{\partial q} \frac{QP_2(\cos\theta)}{r^3} \right] \tag{4}$$

where r is the distance between the electron and the center of the quadrupole when the traceless quadrupole moment tensor is used. It should be noted that the quadrupole moment is a tensor in which the nine elements in the 3 × 3 matrix represent the three-dimensional shape of the QM ellipsoid. The exact

https://dx.doi.org/10.1021/acs.jpclett.1c00169
J. Phys. Chem. Lett. 2021, 12, 1947−1954

expression of the electron−QM interaction potential function is generally nontrivial. Equation 4 is valid only for the specific model system composed by the two opposing dipoles with the same magnitudes.[56] Here, the second Legendre polynomial depicts the angular dependence of the potential energy of the loosely bound electron. It suggests that the potential function is repulsive along the molecule-fixed x-axis connecting the opposing dipoles, whereas it is attractive along the perpendicular y- and z-axes (Figure 3). As such, the potential function is strongly dependent on the polar angle (θ) while it is assumed to be isotropic with respect to the azimuthal angle of ϕ. For the 4-CP radical (Figure 1b, inset), the x-axis could be set to be the molecule-fixed axis connecting the electron-withdrawing O· and CN substituents, though the opposing dipoles are not exactly canceled out. The y- or z-axis is then parallel or perpendicular to the plane of the phenyl moiety, respectively. Although the simple physical model of the two opposing dipoles does not represent the exact potential function describing the electron−QM interaction for the arbitrarily shaped molecule, we may refer eq 4 for the approximate measure of the instant change of the interaction potential of the QBS and its influence on the autodetachment dynamics.

We have carried out *ab initio* calculations for the estimation of the QM derivatives with respect to the normal coordinates. For the $12'^1$ mode, the off-diagonal elements of the derivative tensor are negligibly small whereas the diagonal elements are calculated to be 0.0004, 0.0148, and 0.0186 for $(\partial Q_{xx}/\partial q_{\nu_{12}})$, $(\partial Q_{yy}/\partial q_{\nu_{12}})$, and $(\partial Q_{zz}/\partial q_{\nu_{12}})$, respectively (see Table S2). The derivative QM tensor is then responsible for the instant change in the electron−QM interaction potential along the radial direction, whereas its angular dependence remains intact. According to Fermi's golden rule, the instant radial fluctuation of the QM ellipsoid associated with the $12'^1$ mode, where the extent of the "wobbling" along the radical direction could be roughly estimated from the derivative QM tensor, is responsible for the corresponding autodetachment lifetime of 56 ps (Figures 2 and 3). The autodetachment rate of the $12'^2$ mode ($\tau \sim 27.4 \pm 7.5$ ps), which is 2 times faster than that of the $12'^1$ mode (*vide supra*), could be attributed to the derivative Franck−Condon (FC) factor, $\left\langle \nu_f \left| \frac{\partial}{\partial q} \right| \nu_i \right\rangle$.[30] The $\Delta\nu = -1$ selection rule imposes that the coupling of the nuclear motions of the normal mode to the release of the loosely bound electron is almost identical for both fundamental and overtone modes in terms of the intrinsic nature of the wobbling. The derivative FC factor that is strongly dependent on the vibrational quantum number (n) in the $(n) \rightarrow (n-1)$ transition is then the crucial factor as previously demonstrated in the DBS of the phenoxide anion.[30] The derivative FC factor alone predicts the autodetachment rate of the $12'^2$ mode to be ∼4 times faster than that of the $12'^1$ mode if the harmonic approximation is used for the vibrational wave functions. The anharmonicity of the $12'$ mode of the 4-CP QBS should be one of the reasons why the rate of the $12'^2$ mode is only 2 times faster than that of the $12'^1$ mode, though other energetic parameters affecting the overall autodetachment rate are also slightly different for the two cases.

Interestingly, for the out-of-plane or in-plane bending modes, the off-diagonal elements of the QM tensor are calculated to be non-zero at both positive and negative displacements (see the Supporting Information). The non-zero off-diagonal elements suggest the instantaneous angular displacement of the antiparallel dipolar functional groups from the equilibrium geometry, resulting in the roly poly-like motion of the QM ellipsoid around the specific molecule-fixed principal axis. This could be visualized by the rotational matrix in the diagonalization of the nondiagonal QM tensor. For the $21'^1$ mode, the derivative QM tensor has the non-zero off-diagonal elements. The instant changes of the QM ellipsoid with respect to the polar angle (θ) as well as along the radial direction then significantly influence the autodetachment rate. As depicted in Figure 3, the QM ellipsoid is enforced to be angularly distorted around the y-axis by $21'$ mode excitation. The angular portion of the interaction potential, as represented by the second Legendre polynomial, is extremely sensitive to the polar angle even in the simple physical model. For instance, as the QM ellipsoid tilts toward the x-axis, the electron in the QBS should experience a quite shallow binding potential. In other words, the binding potential declines very rapidly with the increase in the polar angle to accelerate the falloff of the electron.[50] The experimental result giving the dramatically shortened lifetime ($\tau \leq 2.87$ ps) for the $21'^1$ mode could thus be rationalized by the associated angular motion of the QM ellipsoid around the y-axis. The amplitude of the angular oscillation is proportional to the magnitude of the off-diagonal elements, which would also be highly mode-dependent. We have calculated the derivative QM tensors for all FC active vibrational modes (see the Supporting Information). It is interesting to note that the magnitudes of the off-diagonal elements are found to be largest for the $21'$ mode among all FC active modes. The maximum distortion angle of the QM ellipsoid induced by the $21'$ mode excitation is estimated to be ∼11.8° from the rotational matrices in the matrix diagonalization, whereas that associated with the $33'$ mode is calculated to be very small (*vide infra*). The angular distortion of the QM ellipsoid by the vibrational mode excitation is intrinsically different from the rotation of the whole molecule. First, the overall rotation of the whole molecule, especially in the cryogenically cooled condition, is quite slow to give the only very weak coupling strength for the electron−nuclear interaction. Moreover, the electron−QM interaction potential is not supposed to be modified due to the overall rotation of the whole molecule, although it would be a different story when the rotational speed exceeds the vibrational oscillation frequency.

For the 707 cm^{-1} band, two different combination modes of $12'^133'^2$ and $31'^133'^1$ are possible candidates for the mode assignment. The autodetachment lifetime of the 707 cm^{-1} band is measured to be 11.4 ± 3.8 ps, indicating that its autodetachment rate is faster than that of the $12'^1$ mode while it is much slower compared to that of the $21'^1$ mode. Our photoelectron images (Figure 2b) indicate that the major indirect autodetachment process takes place via the vibrational mode of $33'$, resulting in the 31^1 radical being a major product. The $33'$ mode has non-zero off-diagonal elements in the derivative QM tensor, suggesting that the $33'$ mode should be a more efficient wobbler than the $12'$ mode. At the same time, the magnitude of the off-diagonal element of the $33'$ mode is calculated to be much smaller than that of the $21'$ mode, explaining the relatively slower autodetachment rate of the $33'$ mode compared to that of the $21'$ mode. It should also be noted that the wobbling in terms of the angular distortion of the QM ellipsoid could be different in its effectiveness on the autodetachment rate depending on the direction of the angular

https://dx.doi.org/10.1021/acs.jpclett.1c00169
J. Phys. Chem. Lett. 2021, 12, 1947−1954

motion. It was previously proposed that the quadrupole-bound orbital may have a donut shape with a hole along the dipolar axis (x-axis for 4-CP).[32,46] For the 4-CP QBS, therefore, the excess electron is likely to be mostly populated on the plane perpendicular to the x-axis. The angular motion around the x-axis is thus expected to be least efficient with respect to autodetachment as the electron−QM interaction potential is little influenced by the angular motion around the x-axis, which does not exert the extracting force on the loosely bound electron. The vibrational modes of 12′, 14′, or 15′ are calculated to have non-zero off-diagonal elements of D_{yz} and D_{zy}, implying that the angular distortion should be around the x-axis. Due to the spectral congestion, however, those modes could not be identified at present. The exploration of these modes in the near future would be quite interesting to validate the physical model proposed in this work.

The direct comparison of the QBS and DBS in terms of the autodetachment dynamics would be interesting. In Fermi's golden rule, the calculation of energetic parameters such as the vanishing vibrational energy and the kinetic energy of the ejected electron is quite straightforward. The density of states of the ejecting electron (ρ) is proportional to the square root of the electron kinetic energy irrespective of the binding potential.[53] Therefore, the effect of the density of states on the autodetachment rate is estimated to be almost constant for both the phenoxide DBS ($11'^1$ mode)[30] and the 4-CP QBS ($12'^1$ mode). The ratio of the ε_{if} value (eq 3) of the $11'^1$ phenoxide DBS to that of the $12'^1$ 4-CP QBS is calculated to be ∼1.64, suggesting that the autodetachment rate of the DBS is supposed to be slower than that of the QBS. The experimental fact that the autodetachment of the QBS is actually slower than that of the DBS, therefore, might indicate that the coupling of the nuclear motions to the electron binging potential is relatively weaker in the QBS than in the DBS. However, this is an extremely rough estimation, and it may be fair to state that the coupling strengths of the QBS and DBS are roughly of the same order of magnitude from the present perspective based on the comparison of just two typical cases. The most dramatic difference between QBS and DBS dynamics could be rather found in the stereodynamic wobbling mechanism. Namely, the instant three-dimensional topological changes in the QM ellipsoid should be thoroughly characterized before one tries to figure out the mode-specific autodetachment dynamics in the QBS, whereas the derivative of the one-dimensional dipole moment vector seems to dictate the overall autodetachment dynamics of the DBS. Naturally, understanding the QBS dynamics seems to be quite challenging as the three-dimensional topological property of the nuclear motion is intimately related to the release of the loosely bound electron through the complicated stereodynamic electron−QM interaction potentials. The rigorous theoretical treatment of the QBS autodetachment dynamics would be therefore extremely challenging but highly desirable in the near future.

In conclusion, we report here the first real-time autodetachment dynamics of the QBS of the cold anion. Individual vibrational Feshbach resonances above the photodetachment threshold are well identified in the photodetachment spectrum of the cryogenically cooled 4-cyanophenoxide anion. The picosecond time-resolved pump−probe technique combined with the photoelectron velocity-map imaging setup has revealed the state-specific autodetachment rates of the QBS for the first time. The autodetachment rate is found to be dramatically mode-dependent. This dynamic behavior has been explained by the simple physical model in which the three-dimensional QM ellipsoid is wobbled by the vibrational mode according to the derivative QM tensor. The stereodynamic wobbling, especially with respect to the angular coordinates, is particularly efficient in shaking off the loosely bound electron from the QBS as the electron QM tensor potential is highly sensitive to the angular position of the electron with respect to the QM ellipsoid.

EXPERIMENTAL METHODS

Details of the experimental apparatus were described previously.[30] 4-Cyanophenol (1 mM, TCI Chemicals Inc.) was dissolved in the 9:1 methanol/water mixture with a few drops of the ammonia solution. The solution was sprayed by the homemade ESI source with a dissolving voltage of −3000 V. Anions formed from the ESI were introduced into the vacuum chamber with a heated capillary and subsequently transferred into a dual-stage ion funnel (IF141, Masstech). Accumulated anions were then mass-selected and guided into the cryogenically cooled 8 K quadrupole ion trap by a quadrupole mass selector and a series of ion guides (Ardara Technologies). After a trapping time of ∼50 ms, the internally cooled anions were accelerated into the velocity-map imaging apparatus.[57,58] Photoelectrons generated from the interaction between the picosecond laser and anions were collected by the 40 mm diameter position sensitive detector equipped with microchannel plates (MCP) combined with the phosphor screen. Raw photoelectron images were reconstructed by the BASEX program.[59] The schematic of the whole apparatus is depicted in Figure 1. Picosecond pump−probe laser pulses were generated from the 1 kHz picosecond Ti:sapphire regenerative amplifier system (Legend Elite-P, Coherent) seeded with a femtosecond oscillator (Vitara-T-HP, Coherent). A tunable VIS/UV pulse for the pump laser was obtained from the optical parametric amplifier (TOPAS-800 ps, Light Conversion) pumped by the fundamental outputs. The probe pulse was obtained from the fundamental pulse. Both pulses were loosely focused by the CaF_2 plano-convex lenses. The peak powers of both pulses were on the order of $\sim 10^{10}$ W/cm^2. The delay times between the pump and probe laser pulses were controlled by a DC motor-driven optical delay stage (DDS220, Thorlabs) combined with the retro-reflectors (UBBR2.5-1UV, Newport). The photoelectron transients were taken at the magic angle (∼54.7°) between the pump and probe polarization axes.

ASSOCIATED CONTENT

Supporting Information

The Supporting Information is available free of charge at https://pubs.acs.org/doi/10.1021/acs.jpclett.1c00169.

Details of the calculation method for the quadrupole moment upon molecular vibration along with the fitting procedure (PDF)

AUTHOR INFORMATION

Corresponding Author

Sang Kyu Kim − *Department of Chemistry, KAIST, Daejeon 34141, Republic of Korea;* orcid.org/0000-0003-4803-1327; Email: sangkyukim@kaist.ac.kr

https://dx.doi.org/10.1021/acs.jpclett.1c00169
J. Phys. Chem. Lett. 2021, 12, 1947−1954

Authors

Do Hyung Kang − *Department of Chemistry, KAIST, Daejeon 34141, Republic of Korea;* orcid.org/0000-0003-4774-9062

Jinwoo Kim − *Department of Chemistry, KAIST, Daejeon 34141, Republic of Korea*

Min Cheng − *Department of Chemistry, KAIST, Daejeon 34141, Republic of Korea; Beijing National Laboratory for Molecular Sciences, Institute of Chemistry, Chinese Academy of Sciences, Beijing 100190, China; University of Chinese Academy of Sciences, Beijing 100049, China;* orcid.org/0000-0001-5826-5149

Complete contact information is available at: https://pubs.acs.org/10.1021/acs.jpclett.1c00169

Notes

The authors declare no competing financial interest.

■ ACKNOWLEDGMENTS

This work was supported by the National Research Foundation of Korea (2018R1A2B3004534 and 2019R1A6A1A10073887). M.C. acknowledges support from the Korea-China Young Researchers Exchange Program (FY2019).

■ REFERENCES

(1) Fermi, E.; Teller, E. The Capture of Negative Mesotrons in Matter. *Phys. Rev.* **1947**, *72*, 399−408.

(2) Compton, R. N.; Hammer, N. I. *Advancens in Gas-Phase Ion Chemistry*; Adams, N., Babcock, I., Eds.; Elsevier Science: New York, 2001; pp 257−305.

(3) Simons, J. Molecular Anions. *J. Phys. Chem. A* **2008**, *112*, 6401−511.

(4) Tulej, M.; Guthe, F.; Pachkov, M. V.; Tikhomirov, K.; Xu, R.; Jungen, M.; Maier, J. P. Feshbach States of the Propadienylidene Anion H_2CCC^-. *Phys. Chem. Chem. Phys.* **2001**, *3*, 4674−4678.

(5) Guthe, F.; Tulej, M.; Pachkov, M. V.; Maier, J. P. Photodetachment Spectrum of 1-$C_3H_2^-$: The Role of Dipole Bound States for Electron Attachment in Interstellar Clouds. *Astrophys. J.* **2001**, *555*, 466−471.

(6) Verlet, J. R. R.; Anstoter, C. S.; Bull, J. N.; Rogers, J. P. Role of Nonvalence States in the Ultrafast Dynamics of Isolated Anions. *J. Phys. Chem. A* **2020**, *124*, 3507−3519.

(7) Bull, J. N.; Anstoter, C. S.; Verlet, J. R. R. Ultrafast Valence to Non-Valence Excited State Dynamics in a Common Anionic Chromophore. *Nat. Commun.* **2019**, *10*, 5820.

(8) Anstoter, C. S.; Curchod, B. F. E.; Verlet, J. R. R. Geometric and Electronic Structure Probed Along the Isomerisation Coordinate of a Photoactive Yellow Protein Chromophore. *Nat. Commun.* **2020**, *11*, 2827.

(9) Jordan, K. D.; Wang, F. Theory of Dipole-Bound Anions. *Annu. Rev. Phys. Chem.* **2003**, *54*, 367−396.

(10) Simons, J. Theoretical Study of Negative Molecular Ions. *Annu. Rev. Phys. Chem.* **2011**, *62*, 107−128.

(11) Desfrancois, C.; Baillon, B.; Schermann, J. P.; Arnold, S. T.; Hendricks, J. H.; Bowen, K. H. Prediction and Observation of a New, Ground State, Dipole-Bound Dimer Anion: The Mixed Water/Ammonia System. *Phys. Rev. Lett.* **1994**, *72*, 48−51.

(12) Lykke, K. R.; Mead, R. D.; Lineberger, W. C. Observation of Dipole-Bound States of Negative-Ions. *Phys. Rev. Lett.* **1984**, *52*, 2221−2224.

(13) Jagau, T. C.; Bravaya, K. B.; Krylov, A. I. Extending Quantum Chemistry of Bound States to Electronic Resonances. *Annu. Rev. Phys. Chem.* **2017**, *68*, 525−553.

(14) Desfrancois, C.; Abdoul-Carime, H.; Khelifa, N.; Schermann, J. P. From 1/r to $1/r^2$ Potentials: Electron Exchange between Rydberg Atoms and Polar Molecules. *Phys. Rev. Lett.* **1994**, *73*, 2436−2439.

(15) Qian, C. H.; Zhu, G. Z.; Wang, L. S. Probing the Critical Dipole Moment To Support Excited Dipole-Bound States in Valence-Bound Anions. *J. Phys. Chem. Lett.* **2019**, *10*, 6472−6477.

(16) Hammer, N. I.; Diri, K.; Jordan, K. D.; Desfrancois, C.; Compton, R. N. Dipole-Bound Anions of Carbonyl, Nitrile, and Sulfoxide Containing Molecules. *J. Chem. Phys.* **2003**, *119*, 3650−3660.

(17) Sommerfeld, T. Dipole-Bound States as Doorways in (Dissociative) Electron Attachment. *J. Phys.: Conf. Ser.* **2005**, *4*, 245−250.

(18) Kunin, A.; Neumark, D. M. Time-Resolved Radiation Chemistry: Femtosecond Photoelectron Spectroscopy of Electron Attachment and Photodissociation Dynamics in Iodide-Nucleobase Clusters. *Phys. Chem. Chem. Phys.* **2019**, *21*, 7239−7255.

(19) Bull, J. N.; West, C. W.; Verlet, J. R. R. Ultrafast Dynamics of Formation and Autodetachment of a Dipole-Bound State in an Open-Shell π-Stacked Dimer Anion. *Chem. Sci.* **2016**, *7*, 5352−5361.

(20) Anstoter, C. S.; Verlet, J. R. R. Gas-Phase Synthesis and Characterization of the Methyl-2,2-dicyanoacetate Anion Using Photoelectron Imaging and Dipole-Bound State Autodetachment. *J. Phys. Chem. Lett.* **2020**, *11*, 6456−6462.

(21) Liu, G.; Ciborowski, S. M.; Graham, J. D.; Buytendyk, A. M.; Bowen, K. H. Photoelectron Spectroscopic Study of Dipole-Bound and Valence-Bound Nitromethane Anions Formed by Rydberg Electron Transfer. *J. Chem. Phys.* **2020**, *153*, 044307.

(22) Yandell, M. A.; King, S. B.; Neumark, D. M. Time-Resolved Radiation Chemistry: Photoelectron Imaging of Transient Negative Ions of Nucleobases. *J. Am. Chem. Soc.* **2013**, *135*, 2128−2131.

(23) Wang, X. B.; Wang, L. S. Development of a Low-Temperature Photoelectron Spectroscopy Instrument Using an Electrospray Ion Source and a Cryogenically Controlled Ion Trap. *Rev. Sci. Instrum.* **2008**, *79*, 073108.

(24) Yuan, D. F.; Liu, Y.; Qian, C. H.; Kocheril, G. S.; Zhang, Y. R.; Rubenstein, B. M.; Wang, L. S. Polarization of Valence Orbitals by the Intramolecular Electric Field from a Diffuse Dipole-Bound Electron. *J. Phys. Chem. Lett.* **2020**, *11*, 7914−7919.

(25) Yuan, D. F.; Liu, Y.; Qian, C. H.; Zhang, Y. R.; Rubenstein, B. M.; Wang, L. S. Observation of a pi-Type Dipole-Bound State in Molecular Anions. *Phys. Rev. Lett.* **2020**, *125*, 073003.

(26) Zhu, G. Z.; Wang, L. S. High-Resolution Photoelectron Imaging and Resonant Photoelectron Spectroscopy via Noncovalently Bound Excited States of Cryogenically Cooled Anions. *Chem. Sci.* **2019**, *10*, 9409−9423.

(27) Czekner, J.; Cheung, L. F.; Kocheril, G. S.; Wang, L. S. Probing the Coupling of a Dipole-Bound Electron with a Molecular Core. *Chem. Sci.* **2019**, *10*, 1386−1391.

(28) Liu, H. T.; Ning, C. G.; Huang, D. L.; Dau, P. D.; Wang, L. S. Observation of Mode-Specific Vibrational Autodetachment from Dipole-Bound States of Cold Anions. *Angew. Chem., Int. Ed.* **2013**, *52*, 8976−8979.

(29) Liu, H. T.; Ning, C. G.; Huang, D. L.; Wang, L. S. Vibrational Spectroscopy of the Dehydrogenated Uracil Radical by Autodetachment of Dipole-Bound Excited States of Cold Anions. *Angew. Chem., Int. Ed.* **2014**, *53*, 2464−2468.

(30) Kang, D. H.; An, S.; Kim, S. K. Real-Time Autodetachment Dynamics of Vibrational Feshbach Resonances in a Dipole-Bound State. *Phys. Rev. Lett.* **2020**, *125*, 093001.

(31) Sommerfeld, T.; Jordan, K. D. Electron Binding Motifs of $(H_2O)_n^-$ Clusters. *J. Am. Chem. Soc.* **2006**, *128*, 5828−5833.

(32) Sommerfeld, T.; Dreux, K. M.; Joshi, R. Excess Electrons Bound to Molecular Systems with a Vanishing Dipole but Large Molecular Quadrupole. *J. Phys. Chem. A* **2014**, *118*, 7320−7329.

(33) Bull, J. N.; Verlet, J. R. R. Observation and Ultrafast Dynamics of a Nonvalence Correlation-Bound State of an Anion. *Sci. Adv.* **2017**, *3*, No. e1603106.

(34) Rogers, J. P.; Anstoter, C. S.; Verlet, J. R. R. Ultrafast Dynamics of Low-Energy Electron Attachment via a Non-Valence Correlation-Bound State. *Nat. Chem.* **2018**, *10*, 341−346.
(35) Voora, V. K.; Cederbaum, L. S.; Jordan, K. D. Existence of a Correlation Bound s-Type Anion State of C_{60}. *J. Phys. Chem. Lett.* **2013**, *4*, 849−853.
(36) Bezchastnov, V. G.; Vysotskiy, V. P.; Cederbaum, L. S. Anions of Xenon Clusters Bound by Long-Range Electron Correlations. *Phys. Rev. Lett.* **2011**, *107*, 133401.
(37) Ciborowski, S. M.; Harris, R. M.; Liu, G.; Martinez-Martinez, C. J.; Skurski, P.; Bowen, K. H., Jr. The Correlation-Bound Anion of p-Chloroaniline. *J. Chem. Phys.* **2019**, *150*, 161103.
(38) Choi, T. H.; Jordan, K. D. Model Potential Study of Non-Valence Correlation-Bound Anions of $(C_{60})_n$ Clusters: The Role of Electric Field-Induced Charge Transfer. *Faraday Discuss.* **2019**, *217*, 547−560.
(39) Gutowski, M.; Skurski, P.; Li, X.; Wang, L. S. $(MgO)_n^-$ (n = 1−5) Clusters: Multipole-Bound Anions and Photodetachment Spectroscopy. *Phys. Rev. Lett.* **2000**, *85*, 3145−3148.
(40) Abdoul-Carime, H.; Desfrancois, C. Electrons Weakly Bound to Molecules by Dipolar, Quadrupolar or Polarization Forces. *Eur. Phys. J. D* **1998**, *2*, 149−156.
(41) Desfrançois, C.; Périquet, V.; Lyapustina, S. A.; Lippa, T. P.; Robinson, D. W.; Bowen, K. H.; Nonaka, H.; Compton, R. N. Electron Binding to Valence and Multipole States of Molecules: Nitrobenzene, para- and meta-Dinitrobenzenes. *J. Chem. Phys.* **1999**, *111*, 4569−4576.
(42) Liu, G.; Ciborowski, S. M.; Pitts, C. R.; Graham, J. D.; Buytendyk, A. M.; Lectka, T.; Bowen, K. H. Observation of The Dipole- and Quadrupole-Bound Anions of 1,4-Dicyanocyclohexane. *Phys. Chem. Chem. Phys.* **2019**, *21*, 18310−18315.
(43) Liu, Y.; Zhu, G. Z.; Yuan, D. F.; Qian, C. H.; Zhang, Y. R.; Rubenstein, B. M.; Wang, L. S. Observation of a Symmetry-Forbidden Excited Quadrupole-Bound State. *J. Am. Chem. Soc.* **2020**, *142*, 20240−20246.
(44) Compton, R. N.; Dunning, F. B.; Nordlander, P. On the Binding of Electrons to CS_2: Possible Role of Quadrupole-Bound States. *Chem. Phys. Lett.* **1996**, *253*, 8−12.
(45) Liu, G.; Ciborowski, S. M.; Graham, J. D.; Buytendyk, A. M.; Bowen, K. H. The Ground State, Quadrupole-Bound Anion of Succinonitrile Revisited. *J. Chem. Phys.* **2019**, *151*, 101101.
(46) Desfrancois, C.; Bouteiller, Y.; Schermann, J. P.; Radisic, D.; Stokes, S. T.; Bowen, K. H.; Hammer, N. I.; Compton, R. N. Long-Range Electron Binding to Quadrupolar Molecules. *Phys. Rev. Lett.* **2004**, *92*, 083003.
(47) Zhu, G. Z.; Liu, Y.; Wang, L. S. Observation of Excited Quadrupole-Bound States in Cold Anions. *Phys. Rev. Lett.* **2017**, *119*, 023002.
(48) Simons, J. Propensity Rules for Vibration-Induced Electron Detachment of Anions. *J. Am. Chem. Soc.* **1981**, *103*, 3971−3976.
(49) Acharya, P. K.; Kendall, R. A.; Simons, J. Vibration-Induced Electron Detachment in Molecular Anions. *J. Am. Chem. Soc.* **1984**, *106*, 3402−3407.
(50) Simons, J. Ejecting Electrons from Molecular Anions via Shine, Shake/Rattle, and Roll. *J. Phys. Chem. A* **2020**, *124*, 8778−8797.
(51) Yokoyama, K.; Leach, G. W.; Kim, J. B.; Lineberger, W. C. Autodetachment Spectroscopy and Dynamics of Dipole Bound States of Negative Ions: $^2A_1-^2B_1$ Transitions of H_2CCC^-. *J. Chem. Phys.* **1996**, *105*, 10696−10705.
(52) Yokoyama, K.; Leach, G. W.; Kim, J. B.; Lineberger, W. C.; Boldyrev, A. I.; Gutowski, M. Autodetachment Spectroscopy and Dynamics of Vibrationally Excited Dipole-Bound States of H_2CCC^-. *J. Chem. Phys.* **1996**, *105*, 10706−10718.
(53) Neumark, D. M.; Lykke, K. R.; Andersen, T.; Lineberger, W. C. Infrared-Spectrum and Autodetachment Dynamics of NH^-. *J. Chem. Phys.* **1985**, *83*, 4364−4373.
(54) Chalasinski, G.; Kendall, R. A.; Taylor, H.; Simons, J. Propensity Rules for Vibration-Rotation-Induced Electron Detachment of Diatomic Anions: Application to $NH^- \rightarrow NH + e^-$. *J. Phys. Chem.* **1988**, *92*, 3086−3091.
(55) Anstoter, C. S.; Mensa-Bonsu, G.; Nag, P.; Rankovic, M.; Kumar, T. P. R.; Boichenko, A. N.; Bochenkova, A. V.; Fedor, J.; Verlet, J. R. R. Mode-Specific Vibrational Autodetachment Following Excitation of Electronic Resonances by Electrons and Photons. *Phys. Rev. Lett.* **2020**, *124*, 203401.
(56) Ambika Prasad, M. V. N.; Wallis, R. F.; Herman, R. Theory of the Binding Energy of an Electron in the Field of a Linear Electric Quadrupole. *Phys. Rev. B: Condens. Matter Mater. Phys.* **1989**, *40*, 5924−5928.
(57) Chandler, D. W.; Houston, P. L. Two-Dimensional Imaging of State-Selected Photodissociation Products Detected by Multiphoton Ionization. *J. Chem. Phys.* **1987**, *87*, 1445−1447.
(58) Eppink, A. T. J. B.; Parker, D. H. Velocity Map Imaging of Ions and Electrons using Electrostatic Lenses: Application in Photoelectron and Photofragment Ion Imaging of Molecular Oxygen. *Rev. Sci. Instrum.* **1997**, *68*, 3477−3484.
(59) Dribinski, V.; Ossadtchi, A.; Mandelshtam, V. A.; Reisler, H. Reconstruction of Abel-Transformable Images: The Gaussian Basis-Set Expansion Abel Transform Method. *Rev. Sci. Instrum.* **2002**, *73*, 2634−2642.

https://dx.doi.org/10.1021/acs.jpclett.1c00169
J. Phys. Chem. Lett. 2021, 12, 1947−1954